

Collisions in Turbulence: Flow Structures Matter and How

Jason R. Picardo,^{1,*} Lokahith Aghasthya,^{2,†} Rama Govindarajan,^{1,‡} and Samridhhi Sankar Ray^{1,§}

¹*International Centre for Theoretical Sciences, Tata Institute of Fundamental Research, Bangalore 560089, India*

²*Indian Institute for Science Education and Research, Pune 411008, India*

The role of the spatial structure of a turbulent flow in enhancing particle collision rates in suspensions is an open question. We show and quantify, as a function of particle inertia, the correlation between the multiscale structures of turbulence and particle collisions: Straining zones contribute predominantly to rapid head-on collisions compared to vortical regions. We also discover the importance of vortex-strain worm-rolls, which goes beyond ideas of preferential concentration and may explain the rapid growth of aggregates in natural processes, such as the initiation of rain in warm clouds.

Turbulence is riddled with a hierarchy of interacting vortical and straining structures (Fig. 1), which are closely related to its characteristic intermittent and non-Gaussian statistics [1–6]. The most intense structures typically occur near each other, in the form of vortex tubes surrounded by straining sheets, as shown in Fig. 1. This organization—a sort of vortex-strain *worm-rolls*—is characteristic of turbulent flows [7–10], and its origin and dynamical implications continue to be investigated [11–16]. These structures distinguish fully developed turbulence from purely random flow fields, and must play an important role in many aspects of turbulent transport. The most important of these—because it remains central to our understanding of phenomena as diverse as the formation of planets in circumstellar disks [17] or the initiation of rain in warm clouds [18, 19]—is the growth of macroscopic aggregates, due to collisions and coalescences, from nuclei-particles (dust or aerosols) suspended in a turbulent flow. The role of the underlying turbulent carrier flow is critical: Estimates of, e.g., the rate of growth of these aggregates in the absence of such flows do not agree with that seen in nature [20]. Indeed, the explanation of such rapid growth through coalescence, demonstrated [21–23] and quantified in terms of flow statistics [20, 24, 25], is rooted in the ability of turbulent flows to enhance the rate of collisions between nuclei seed-particles.

A critical discovery, due to Bec, *et al.* [22], was to find the precise connection between the intermittent (multi-scaling) nature of the carrier turbulent flow and the accelerated growth of aggregates. And yet the implied correlation between the structure of the flow and droplet collisions-coalescences remains unknown. Indeed, there is evidence to suggest that flow structures matter. But the question is how and when?

In this paper we answer this question comprehensively, based on detailed state-of-the-art direct numerical simulations (DNSs), and show how straining regions are intrinsically more effective at generating collisions than vortical ones even for uniformly distributed *inertia-less* particles. Particle inertia widens this discrepancy, not simply by preferential concentration, but also by selectively increasing the collision velocities in straining zones.

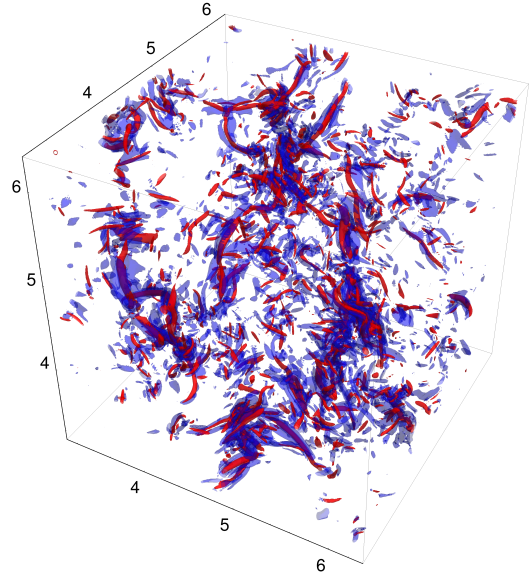


FIG. 1. A representative snapshot of three-dimensional contours of Q showing intense vortex tubes (opaque red: $+5.6\sqrt{\langle Q^2 \rangle}$) enveloped by dissipative, straining sheets (transparent blue: $-2\sqrt{\langle Q^2 \rangle}$).

This is because straining regions have a larger proportion of *head-on* or *rear-end* collisions, as opposed to *side-on* collisions, which are predominant in vortical regions. Consequently, a larger fraction of the velocity gradient in straining zones is translated into the particle approach velocity. Finally, and most strikingly, we show how intense vorticity and strain, cohabiting as vortex-strain *worm-rolls*, conspire to generate rapid, violent collisions.

We therefore consider a turbulent flow whose velocity \mathbf{u} (subject to the incompressibility constraint $\nabla \cdot \mathbf{u} = 0$) is a solution to the Navier-Stokes equation

$$\partial_t \mathbf{u} + (\mathbf{u} \cdot \nabla) \mathbf{u} = -\nabla p + \nu \nabla^2 \mathbf{u} + \mathbf{f} \quad (1)$$

where ν is the kinematic viscosity. We perform DNSs on a tri-periodic domain with $N^3 = 512^3$ grid points, by using a standard de-aliased pseudo-spectral solver [26] and a second-order Adams-Bashford scheme for time integration. A statistically stationary, homogeneous and

isotropic flow is maintained by the time-dependent large-scale forcing \mathbf{f} , which injects a constant amount of energy into the first two wavenumber shells. This forcing scheme enables us to control the time-averaged energy dissipation ϵ , which is chosen such that the Kolmogorov length $\eta = (\nu^3/\epsilon)^{1/4}$ satisfies $\eta k_{\max} \approx 1.7$ (where $k_{\max} = \sqrt{2}N/3$ is the maximum resolved wavenumber). The Taylor-Reynolds number ($Re_\lambda = 2E\sqrt{5}/(3\nu\epsilon)$, where E is the total kinetic energy) of the flow is 196.

To identify vortical and straining structures in the flow, we use the \mathcal{Q} criterion [27–29] through the velocity gradient tensor $\mathcal{A} = \tau_\eta \nabla \mathbf{u}$ (normalized by the Kolmogorov time $\tau_\eta = (\nu/\epsilon)^{1/2}$) which yields the symmetric strain rate tensor $\mathcal{S} = (\mathcal{A} + \mathcal{A}^T)/2$ and the anti-symmetric rotation rate tensor $\mathcal{R} = (\mathcal{A} - \mathcal{A}^T)/2$. To compare the relative magnitudes of strain and rotation, we define $S^2 = \mathcal{S}_{ij}\mathcal{S}_{ij}$ and $R^2 = \mathcal{R}_{ij}\mathcal{R}_{ij}$, the difference of which is related to the second invariant of the velocity gradient tensor: $\mathcal{Q} = (R^2 - S^2)/2$. Regions where $\mathcal{Q} < 0$ are dominated by irrotational strain, while regions where $\mathcal{Q} > 0$ are vortical. Near-zero values of \mathcal{Q} may correspond to zones with weak velocity gradients, or to strong shear layers where $R^2 \approx S^2$ [25]. Figure 1 presents contours of large positive and negative values of \mathcal{Q} , which reveal characteristic vortex-strain worm-rolls.

We introduce in the flow 10^6 identical particles, each having a sub-Kolmogorov radius $a = \eta/3$ (we have checked that the results reported here are consistent for smaller radii as well, up to $\eta/10$) and a density ρ_p much larger than that of the carrier-fluid ρ_f . The particles occupy a small volume fraction of $\mathcal{O}(10^{-4})$ and their influence on the flow is negligible. Since the Reynolds number associated with their slip velocities is small, the evolution of particle trajectories $\mathbf{X}_p(t)$ is determined by the simplified Maxey-Riley equations [30]:

$$\frac{d\mathbf{X}_p}{dt} = \mathbf{V}_p, \quad \frac{d\mathbf{V}_p}{dt} = -\frac{1}{\tau_p}[\mathbf{V}_p - \mathbf{u}(\mathbf{X}_p, t)] \quad (2)$$

where $\tau_p = 2a^2\rho_p/(9\nu\rho_f)$, the particle relaxation time, yields the Stokes number ($St = \tau_p/\tau_\eta$), which provides a non-dimensional measure of the particle's inertia. We consider several families of particles, with St ranging from 0 to 16.75. For non-zero St , Eqs. (2) are solved by using an exponential integration scheme [31]. The case of tracers $St = 0$ is handled separately, by directly setting $\mathbf{v}_p(t) = \mathbf{u}(\mathbf{X}_p(t), t)$ and by using a second order Runge-Kutta time-stepper. The fluid velocity at the particle position is obtained via fourth-order B-spline interpolation [32].

After the randomly-seeded particles have settled into a statistically stationary distribution, we begin detecting collisions using an algorithm similar to that in Ref. [21]. We use the standard *ghost collisions* approximation—ignoring coalescence and other post-collision outcomes—to focus on the role of flow structures in bringing particles together and enhancing collision rates.

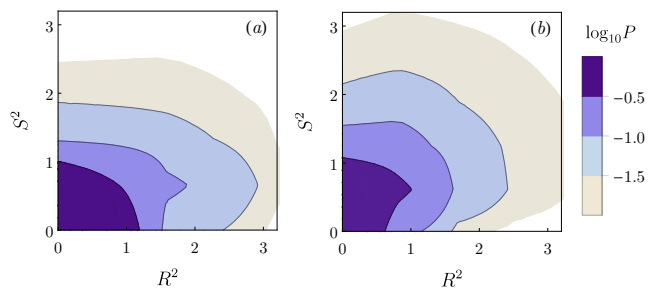


FIG. 2. Bi-probability distribution functions $P(R^2, S^2)$ for inertia-less (tracer) particles, corresponding to the values of R^2 and S^2 sampled by (a) particles and (b) collision locations, which show the disproportionate bias towards collisions in strain-dominated regions.

The rate of collisions depends, of course, on the relative velocity of particles at contact [33–35]. For tracers ($St = 0$) or nearly-tracer particles ($St \gtrsim 0$), this is determined by fluid velocity gradients ($\propto \tau_\eta^{-1}$), which increase in magnitude as the flow becomes more turbulent. This picture, underlying the seminal work of Saffman and Turner [36], is blind to flow structures: It disregards whether the local velocity gradient arises from rotation or strain.

Inertial particles ($St > 0$), e.g., droplets in air, do not respond instantaneously to changes in the flow. Such particles *preferentially concentrate*, thereby increasing their local number density [21]. They can also attain relative velocities much larger than that of the underlying flow. Dubbed the *sling effect* [37], these events correspond to the formation of singularities or *caustics* in the particle velocity field [38, 39]. Although clustering and caustics have been tied to the centrifugal ejection of heavy particles out of vortices, they also occur in smooth random flows that are devoid of structure [40–44]. Consequently, the presence of these effects does not necessarily imply that collisions sense the structures of turbulence.

To unambiguously determine the influence of the local flow field, we must begin with tracers which remain uniformly distributed in space. To allow for collisions, the radii of these particles are kept (artificially) finite, while their inertia is ignored. According to the Saffman-Turner theory [36], collisions should occur uniformly between any two regions that possess the same velocity gradient magnitude, regardless of whether these regions are vortical or straining. We now examine this hypothesis, bearing in mind that a discrepancy will implicate flow structures that are intrinsically more effective at causing collisions.

Towards this end, we calculate the values of R^2 and S^2 along particle trajectories, as well as at collision locations. The results for inertia-less particles are presented as joint probability distributions functions $P(R^2, S^2)$ in Fig. 2a and Fig. 2b, respectively. It is immediately clear

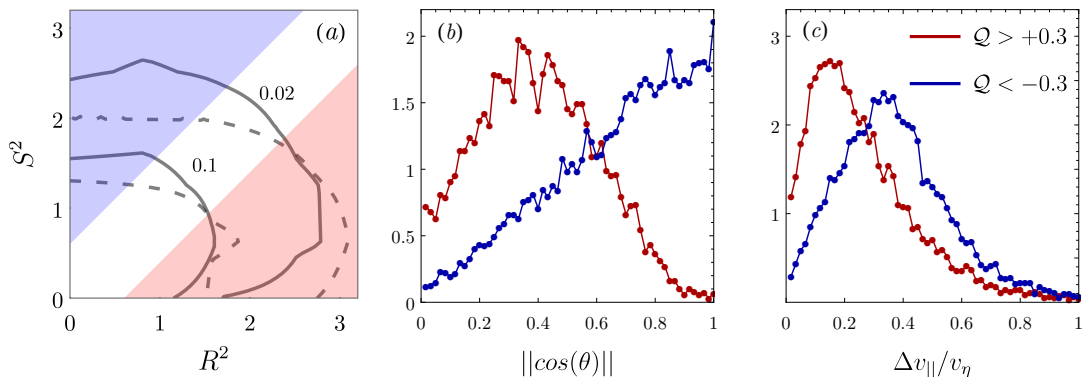


FIG. 3. (a) Contours corresponding to $P(R^2, S^2) = 0.02, 0.1$, sampled by inertia-less particles (dashed) and their collisions (solid). The blue and red shaded portions correspond to $Q < -0.3$ and $Q > +0.3$, and indicate regions dominated by strain and vorticity, respectively. (b) Conditional probability distributions of the cosine of the angle of collision θ , for data corresponding to the shaded portions of panel (a). (c) Conditional probability distributions of the approach velocity at collision $\Delta v_{||}$, normalized by the Kolmogorov velocity v_η . This set of representative plots clearly illustrate why straining regions are more effective at generating collisions.

that collisions under-sample vortical regions ($R^2 > S^2$) and over-sample straining regions ($S^2 > R^2$), relative to where particles reside. This is also seen in Fig. 3a, which overlays contours of $P(R^2, S^2) = 0.1$ and 0.02 , for particles (dashed) and collisions (solid). The strain (vorticity) dominated portion of this plot is shaded in blue (red), and corresponds to $Q < -0.3$ ($Q > +0.3$).

This surprising result is an outcome of the distinct flow topologies of these regions which cause particles to approach each other differently. Fig. 3b presents the distribution of the cosine of the collision angle (θ), for straining (blue) and vortical (red) regions. θ is defined as the angle between the relative velocity vector ($V_{p1} - V_{p2}$) and the separation vector ($X_{p1} - X_{p2}$) at collision. Particles in straining regions tend to collide in a head-on or rear-end manner ($\theta \approx 0$ or π). In either case, a large fraction of the velocity difference between particles contributes to their rate of approach or collision velocity ($\Delta v_{||}$). On the other hand, particles in vortices undergo collisions that are closer to being side-on, in which case the separation vector is nearly perpendicular to the relative velocity. This results in lower approach velocities in vortical regions, as shown in Fig. 3c. Consequently, over a given time interval, fewer particles will collide in vortical regions compared to straining regions with the same magnitude of the velocity gradient and particle number density.

How does particle inertia affect this picture? Figure 4a presents the average value of Q sampled by particles (dashed-red) and their collision locations (solid-black) as a function of St . At $St = 0$, $\langle Q \rangle$ is 0 for particles and -0.04 for collisions. Remarkably, this offset is strongly amplified by inertia and reaches a maximum around $St \approx 0.3$, beyond which particles begin to decouple from the underlying flow and eventually collide

uniformly. The preference of *inertial* particles ($St > 0$) to collide in straining regions has been reported previously by Perrin and Jonker [45, 46]. Our results demonstrate that this effect is not fundamentally tied to particle inertia, but rather is an amplification of a difference that exists even for inertia-less tracers, raising the question: how does particle inertia selectively enhance collisions in straining regions?

One possible explanation is provided by preferential concentration: Heavy particles are centrifuged out of rotational regions, and thus tend to accumulate in straining zones just outside vortices [39]. This causes the number density to increase in straining regions, at the expense of vortical zones, as shown in Fig. 4b. Here, n is a coarse-grained number density, obtained by dividing the domain into bins of size 20η . The average Q in each bin is used to distinguish between vortical ($Q > 0$) and straining regions ($Q < 0$) and obtain the conditionally averaged number density. All else being equal, higher number densities imply larger collision rates [20]. However, we see that the maximum difference in number densities occurs near $St \approx 1$, which is *not* where the maximum difference in $\langle Q \rangle$ is seen (Fig. 4a). Hence another mechanism must be involved.

Inertia is also known to increase the relative velocity between neighboring particles [34, 35], which should result in higher collision velocities. On examining this effect in straining and vortical regions separately, we find that it is stronger in straining regions and, in fact, has no impact on vortical regions for small St . This is demonstrated in Fig. 4c, which presents the average values of $\Delta v_{||}$, conditioned on Q . It appears that head-on (or rear-end) collisions, which prevail in straining zones, are more amenable to being sped-up by inertia than side-on collisions. Notably, the maximum difference between collision

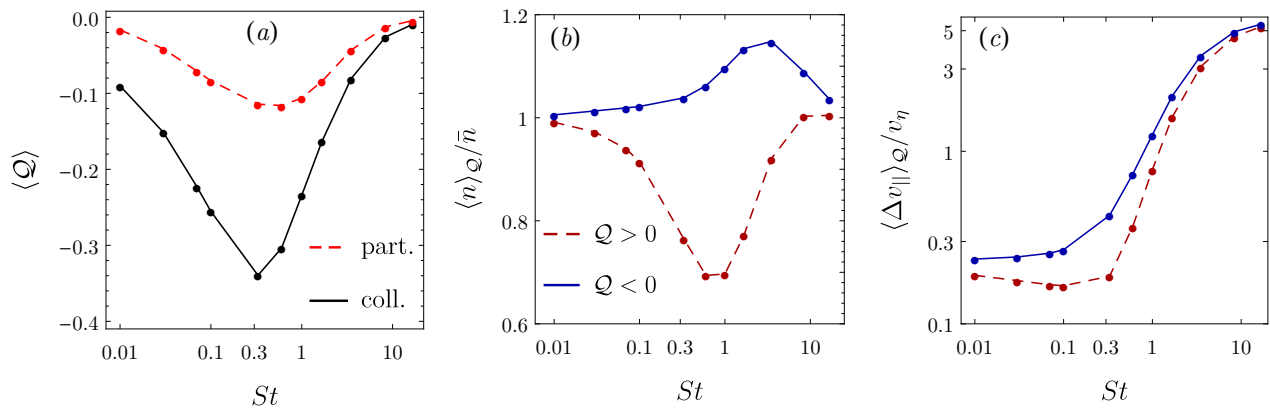


FIG. 4. (a) Average \mathcal{Q} , sampled by particles (red-dashed) and collisions (black-solid), as a function of St . (b) Average particle number density in vortical and straining regions (positive and negative \mathcal{Q}), plotted as a function of St , and normalized by the domain-average number density \bar{n} . (c) Average approach velocity for collisions in vortical and straining regions, normalized by v_η

velocities occurs near $St \approx 0.3$, which matches well with the maximum difference in $\langle \mathcal{Q} \rangle$ (Fig. 4a). Thus, larger approach rates, rather than number densities, appear to be the primary reason for the effectiveness of straining regions in creating collisions.

Thus far, we have considered vortical and straining regions individually. Particle inertia, however, permits structures within a distance of $\tau_p V_p$ to influence a collision. This raises the possibility of vortical and straining regions conspiring to enhance collisions, especially for moderately large St . For example, the geometry of vortex-strain *worm-rolls* (Fig. 1) will cause particles in intense vortex tubes to be rapidly ejected into strong straining sheets, where they are very likely to collide.

We search for evidence of this effect by tracing, backward in time, all particles that collide in straining regions. For the subset that do have at least one particle originating from a vortex, we record (i) the time taken to collide after leaving the vortex and entering the straining zone (t_{strain}), as indicated by \mathcal{Q} changing sign; (ii) the strength of the vortex, measured in terms of the maximum positive value of \mathcal{Q} sampled inside the vortex (\mathcal{Q}_{vortex}); (iii) the intensity of straining at the collision location (\mathcal{Q}_{col}); and (iv) the collision velocity. While measuring the vortex strength, we only back-track for a time of $3\tau_\eta$ within the vortex, to ensure that the \mathcal{Q} values obtained are relevant to the subsequent collision. The conclusions are insensitive to the exact value of this threshold.

Fig. 5 presents the results of this Lagrangian calculation, conditionally averaged on t_{strain} , for $St = 1, 0.6$ and 0.1 . The data for moderately large St (1 and 0.6), reveal the impact of vortex-strain worm-rolls. Particles that collide quickly (small t_{strain}), are found to originate from more intense vortices (Fig. 5a) and to collide in stronger straining regions (Fig. 5b). This signature

weakens considerably for less inertial ($St = 0.1$) particles which are mildly ejected and relax faster to the local straining flow.

The collision velocities for small t_{strain} are also systematically larger (Fig. 5c). The standard deviation about each data point (not shown for clarity) is of the order of the average value. Thus, several small t_{strain} collisions have very large collision velocities, indicative of caustics/sling events, which are known to dominate the collision rate for $St > 0.5$ [20, 24]. Traditionally, these have been linked to rapid ejection from vortices [37]. Our results indicate that this is only half the story: Straining sheets which envelope strong vortices also contribute to generating violent collisions and enhancing collision rates.

An appreciation for flow structures naturally leads one to ask how collisions are affected when structures change. The influence of Re_λ is particularly important to consider, as the estimated values for natural flows are orders of magnitude larger than what can be attained in simulations [17, 18]. Increasing Re_λ results in higher intermittency, which translates into more intense structures (see, e.g., Ref. [47] for a similar study of a model stretched-vortex), but which occupy smaller volumes. These competing effects are known to produce a non-monotonic variation of particle clustering [48]. Regarding collisions, our initial calculations show that differences between vortical and straining regions increase from $Re_\lambda = 69$ to 196; it remains to be seen in a systematic way how this phenomenon is affected in a higher Reynolds number flow.

Flow structures can also be significantly modified by new physical interactions, for example, condensation of water vapour on cloud droplets, which releases latent heat and energizes small scales [49], and elastic feedback from polymers that suppresses small-scale motions [50, 51]. Studying collisions in these complex flows is an

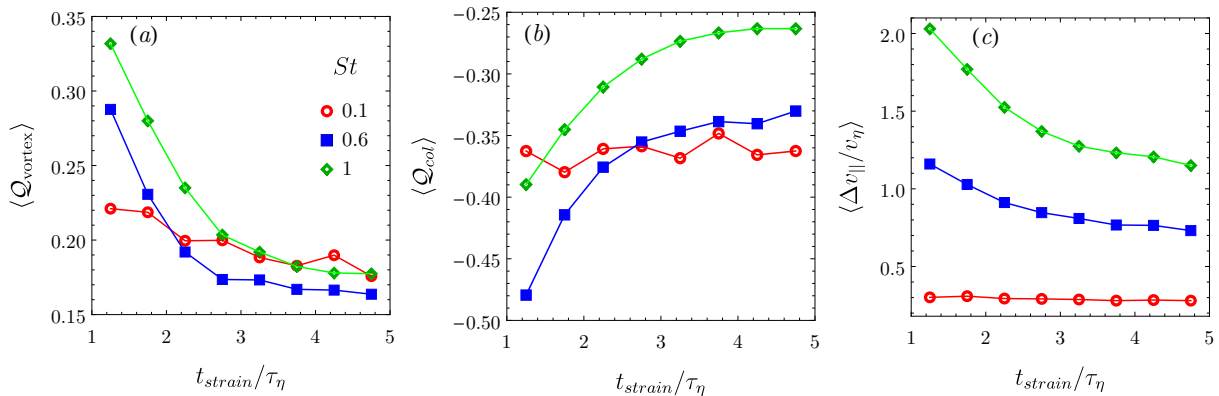


FIG. 5. Representative plots of (a) the maximum value of Q sampled by the particle inside the vortex; (b) the average value of Q at collision; and (c) the corresponding approach velocity at collisions obtained from Lagrangian tracking of particles that collide in straining regions ($Q < 0$) after leaving a vortex and conditionally averaged on the time taken to collide after entering the straining region (t_{strain}). These plots clearly illustrate the singular importance of vortex-strain worm-rolls as discussed in the text.

interesting avenue for future work.

Before we conclude, it is essential to place our work in the context of turbulent transport problems—a canonical example being that of rain-initiation in warm clouds—which have application across the areas of non-equilibrium statistical physics, geophysics, oceanography, astrophysics and atmospheric sciences. Understanding these problems demands not only an appreciation of how fast droplets sediment, collide and coalesce (in which tremendous advances have been made in recent years) but also knowledge of *where* such processes are most likely to occur. This paper, therefore, contributes to a fuller understanding of this question.

We thank Jérémie Bec, S. Ravichandran and Sidhartha Mukherjee for useful suggestions and discussions, which were facilitated in part by a program organized at ICTS: *Turbulence from Angstroms to Light Years* (ICTS/Prog-taly2018/01). The simulations were performed on the ICTS clusters *Mowgli* and *Mario* as well as the work stations from the project ECR/2015/000361: *Goopy* and *Bagha*. SSR acknowledges DST (India) project ECR/2015/000361 for financial support.

* jrpicardo@icts.res.in; picardo21@gmail.com

† lokahith.agasthya@students.iiserpune.ac.in

‡ rama@icts.res.in

§ samriddhisankarray@gmail.com

- [1] U. Frisch, *Turbulence: The legacy of A N Kolmogorov* (Cambridge University Press, Cambridge, UK, 1996).
- [2] A. Tsinober, *An informal conceptual introduction to turbulence* (Springer, New York, USA, 2009).
- [3] J. Schumacher, R. M. Kerr, and K. Horiuti, “Structure and dynamics of vorticity in turbulence,” in *Ten Chapters in Turbulence*, edited by P. A. Davidson, Y. Kaneda, and K. R. Sreenivasan (Cambridge University Press, 2012) p.

4386.

- [4] U. Frisch, A. Pomyalov, I. Procaccia, and S. S. Ray, *Phys. Rev. Lett.* **108**, 074501 (2012).
- [5] M. Buzdicotti, A. Bhatnagar, L. Biferale, A. S. Lanotte, and S. S. Ray, *New J. Phys.* **18**, 113047 (2016).
- [6] A. S. Lanotte, S. K. Malapaka, and L. Biferale, *Eur. Phys. J. E* **39**, 49 (2016).
- [7] B. W. Zeff, D. D. Lanterman, R. McAllister, R. Roy, E. J. Kostelich, and D. P. Lathrop, *Nature* **34**, B479 (2003).
- [8] R. Pandit, P. Perlekar, and S. S. Ray, *Pramana-Journal of Physics* **73**, 157 (2009).
- [9] J. Schumacher, B. Eckhardt, and C. R. Doering, *Phys. Lett. A* **374**, 861 (2010).
- [10] P. Gotzfried, B. Kumar, R. A. Shaw, and J. Schumacher, *J. Fluid Mech.* **814**, 452483 (2017).
- [11] M. Guala, A. Liberzon, A. Tsinober, and W. Kinzelbach, *J. Fluid Mech.* **574**, 405427 (2007).
- [12] P. E. Hamlington, J. Schumacher, and W. J. A. Dahm, *Phys. Rev. E* **77**, 026303 (2008).
- [13] S. S. Ray, *Pramana-Journal of Physics* **84**, 395 (2015).
- [14] M. Wilczek, *J. Fluid Mech.* **784**, 14 (2015).
- [15] J. M. Lawson and J. R. Dawson, *J. Fluid Mech.* **780**, 6098 (2015).
- [16] S. S. Ray, *Phys. Rev. Fluids (Rapid)* **18**, 072601(R) (2018).
- [17] J. J. Lissauer, *Annu. Rev. Astron. and Astrophys.* **31**, 129 (1993).
- [18] W. W. Grabowski and L.-P. Wang, *Annu. Rev. Fluid Mech.* **45**, 293 (2013).
- [19] S. Chen, M.-K. Yau, P. Bartello, and L. Xue, *Atmos. Chem. Phys.* **18**, 7251 (2018).
- [20] A. Pumir and M. Wilkinson, *Annu. Rev. Condens. Ma. P.* **7**, 141 (2016).
- [21] S. Sundaram and L. R. Collins, *J. Fluid Mech.* **335**, 75109 (1997).
- [22] J. Bec, S. S. Ray, E. W. Saw, and H. Homann, *Phys. Rev. E* **93**, 031102(R) (2016).
- [23] R. Onishi, K. Matsuda, and K. Takahashi, *J. Atmos. Sci.* **72**, 2591 (2015).
- [24] M. Voßkuhle, A. Pumir, E. Lévêque, and M. Wilkinson, *J. Fluid Mech.* **749**, 841852 (2014).

- [25] P. J. Ireland, A. D. Bragg, and L. R. Collins, *J. Fluid Mech.* **796**, 617658 (2016).
- [26] C. Canuto, M. Y. Hussaini, A. Quarteroni, and T. A. Zang, *Spectral methods: fundamental in single domains* (Springer-Verlag, Berlin, Germany, 2006).
- [27] Y. Dubief and F. Delcayre, *J. Turbul.* **1**, N11 (2000).
- [28] H. M. Blackburn, N. N. Mansour, and B. J. Cantwell, *J. Fluid Mech.* **310**, 269292 (1996).
- [29] M. S. Chong, A. E. Perry, and B. J. Cantwell, *Phys. Fluids A* **2**, 765 (1990).
- [30] S. Ravichandran, P. Deepu, and R. Govindarajan, *Sādhanā* **42**, 597 (2017).
- [31] P. J. Ireland, T. Vaithianathan, P. S. Sukheswalla, B. Ray, and L. R. Collins, *Comput. Fluids* **76**, 170 (2013).
- [32] M. A. T. van Hinsberg, J. H. M. T. Boonkamp, F. Toschi, and H. J. H. Clercx, *SIAM J. Sci. Comput.* **34**, B479 (2012).
- [33] A. Bhatnagar, K. Gustavsson, B. Mehlig, and D. Mitra, *ArXiv e-prints* (2018), arXiv:1809.10440.
- [34] E.-W. Saw, G. P. Bewley, E. Bodenschatz, S. S. Ray, and J. Bec, *Phys. Fluids* **26**, 111702 (2014).
- [35] M. James and S. S. Ray, *Sci. Rep.* **7**, 12231 (2017).
- [36] P. G. Saffman and J. S. Turner, *J. Fluid Mech.* **1**, 1630 (1956).
- [37] G. Falkovich, A. Fouxon, and M. G. Stepanov, *Nature* **419**, 151 (2002).
- [38] M. Wilkinson, B. Mehlig, and V. Bezuglyy, *Phys. Rev. Lett.* **97**, 048501 (2006).
- [39] S. Ravichandran and R. Govindarajan, *Phys. Fluids* **27**, 033305 (2015).
- [40] J. Bec, A. Celani, M. Cencini, and S. Musacchio, *Phys. Fluids* **17**, 073301 (2005).
- [41] M. Wilkinson, B. Mehlig, S. Östlund, and K. P. Duncan, *Phys Fluids* **19**, 113303 (2007).
- [42] J. Bec, M. Stefano, and S. S. Ray, *Phys. Rev. E* **87**, 063013 (2013).
- [43] K. Gustavsson and B. Mehlig, *Phys. Rev. E* **87**, 023016 (2013).
- [44] K. Gustavsson and B. Mehlig, *J. Turbul.* **15**, 34 (2014).
- [45] V. E. Perrin and H. J. J. Jonker, *Phys. Rev. E* **89**, 033005 (2014).
- [46] V. E. Perrin and H. J. J. Jonker, *J. Fluid Mech.* **792**, 3649 (2016).
- [47] L. Agasthya, J. R. Picardo, S. Ravichandran, R. Govindarajan, and S. S. Ray, *arXiv e-prints* (2018), arXiv:xxxx.xxxx.
- [48] R. Onishi and J. C. Vassilicos, *J. Fluid Mech.* **745**, 279299 (2014).
- [49] S. Ravichandran and R. Govindarajan, *J. Fluid Mech.* **832**, 745776 (2017).
- [50] A. Liberzon, M. Guala, W. Kinzelbach, and A. Tsinober, *Phys. Fluids* **18**, 125101 (2006).
- [51] P. Perlekar, D. Mitra, and R. Pandit, *Phys. Rev. E* **82**, 066313 (2010).